

THE MOTT TRANSITION IN INFINITE DIMENSIONS: OLD IDEAS AND SOME SURPRISES

Gabriel Kotliar and Marcelo J. Rozenberg*

Department of Physics, Rutgers University, Piscataway, NJ 08855, USA

Abstract

The Mott transition phenomena can be studied systematically in the limit of large dimensions. We describe recent results and new insights in this field.

1. Introduction

The Mott transition, namely the metal insulator transition induced by the electron-electron interactions in a periodic system, has been investigated theoretically and experimentally for many years [1]. Experimentally it is realized in transition metal oxides such as V_2O_3 and NiI_2 and can be driven by varying pressure, temperature and composition. The Mott transition inspired the development of many important theoretical concepts. Hubbard introduced the notion of Hubbard bands, and viewed the metal insulator transition as a gradual merging of these bands as the correlation is decreased. Brinkman and Rice viewed the metal insulator transition as a result of a collapse of the Fermi energy or the divergence of the effective mass at a critical value of the interaction U . In this framework the metal insulator transition is driven by the disappearance of the Fermi liquid quasiparticles. Slater pointed out that the metal insulator transition is always accompanied by long range antiferromagnetic order, and viewed the doubling of the unit cell which makes the band structure of the system that of a band-insulator, as the driving force behind the metal insulator transition.

These ideas and the relevance of the Hubbard model as a simple model to account for the essential features displayed by real systems have been debated for a long time.

The interest in the quantum many body problem in the limit of infinite dimensions [2], has led to a new mean field theory of the strong correlation problem [3, 4, 5]. This theory is similar in spirit to the Weiss mean field theory in classical statistical mechanics. It has given new insights into the Mott transition problem [6, 7, 8, 9, 10] and describes quantitatively some recent experiments on three dimensional transition metal oxide systems [10]. We will review here some of these developments.

*©1994 in image and content by the author. Reproduction of this article, by any means, is permitted for non-commercial purposes.

Our starting point is the Hubbard Model:

$$H = - \sum_{\langle i,j \rangle} (t_{ij} + \mu) c_{i\sigma}^\dagger c_{j\sigma} + U \sum_i (n_{i\uparrow} - \frac{1}{2})(n_{i\downarrow} - \frac{1}{2}), \quad (1)$$

where summation over repeated spin indices is assumed.

In the limit of the coordination number m going to infinity, the hopping matrix elements can be chosen to give a semicircular density of states of width $4t$, and are scaled as $t_{ij} \sim \frac{t}{\sqrt{m}}$ [2] to give a well defined and non trivial limit. This density of states is realized on lattices with different amounts of magnetic frustration such as the Bethe lattice (no frustration), the fully connected - fully frustrated lattice (FF) [6, 9], and the two sublattice fully frustrated model (TSFF), which provides a varying degree of frustration [10].

These models are defined as follows: on the Bethe lattice the parameters t_{ij} for $n.n.$ hopping are chosen equal to a constant t . On the fully frustrated lattice, the t_{ij} are chosen as a random variable with gaussian distribution, with zero mean and variance equal to t^2 . In the third model we consider two sublattices. Each one fully connected, with hopping parameters chosen as in the previous case, but with variance equal to t_1^2 .

The hopping between sites on the different sublattices is given by $t_2 = \sqrt{t^2 - t_1^2}$. Magnetic frustration is essential for the Mott phenomena and the study of lattices with varying degrees of frustrations allowed us to understand the interplay of the metal insulator transition and magnetic order.

2. Methodology

The essential idea of the mean field approach is to replace the quantum many body problem by an impurity model in an effective medium which is solved for self consistently.

For the Hubbard model the associated impurity model is an Anderson model defined by the effective action [3]:

$$S_{eff}[c, c^\dagger] = \sum_\sigma \int d\tau d\tau' c_\sigma^\dagger(\tau) G_0^{-1}(\tau - \tau') c_\sigma(\tau') + U \int_0^\beta d\tau (n_{i\uparrow}(\tau) - \frac{1}{2})(n_{i\downarrow}(\tau) - \frac{1}{2}). \quad (2)$$

The propagator G_0 plays the role of a Weiss field and, restricting to the paramagnetic phase (or for the FF model), obeys the self-consistency condition:

$$G_0^{-1}(i\omega_n) = i\omega_n + \mu - t^2 G(i\omega_n) \quad (3)$$

where $G(i\omega_n) = - \int_0^\beta e^{i\omega_n \tau} \langle T_\tau c(\tau) c^\dagger(0) \rangle_{S_{eff}}$ is the local Green function of the Hubbard model once self-consistency is attained.

The mean field approach can also be used to investigate the occurrence of magnetic long range order [4]. To allow for an antiferromagnetic state on a bipartite lattice such as the Bethe lattice, the local Green functions and the Weiss fields are allowed to be spin dependent $G_{A\sigma} = G_{B-\sigma}$. This results in a different self-consistency condition:

$$G_{0A\sigma}^{-1} = i\omega + \mu - t^2 G_{B\sigma} \quad (4)$$

$$G_{0B\sigma}^{-1} = i\omega + \mu - t^2 G_{A\sigma} \quad (5)$$

where A denotes one sublattice and B the other. The two local Green functions G_A and G_B are evaluated independently given $G_{0A\sigma}$, $G_{0B\sigma}$ and the single site action S defined above.

The TSFF model that actually interpolates between the previous two, has a self-consistency condition that reads

$$G_{0A\sigma}^{-1} = i\omega + \mu - t_1^2 G_{A\sigma} - t_2^2 G_{B\sigma} \quad (6)$$

$$G_{0B\sigma}^{-1} = i\omega + \mu - t_1^2 G_{B\sigma} - t_2^2 G_{A\sigma} \quad (7)$$

This model mimics a partial degree of frustration; it reduces to the Bethe lattice when $t_1 = 0$ and to the FF when $t_1 = t_2$.

The mean field equations are coupled functional equations to be solved for the Weiss field G_0 and the local Green function. The most difficult aspect of the mean field theory is the solution of the Anderson impurity model in an arbitrary bath. This class of problems has been studied intensively in the last 40 years and we will draw on this knowledge to make exact and approximate statements on the solution of the lattice model in large dimensions. The essential insight is to use *reliable* approximations to calculate $G\{G_0\}$ in eq. (2), this step captures the local aspects of the problem. The self-consistency condition (3) then brings back the lattice aspect.

Several techniques have been used in the analysis of the mean field equations. They range from qualitative arguments and analytic perturbative schemes to numerical methods based on quantum Montecarlo (QMC) [11, 6, 7], exact diagonalization (ED) [12, 13, 14] and second order perturbative calculations (2OPT) [3, 8, 9, 10]. To obtain details of the low energy behavior we have developed the projective self-consistent method which is the lattice equivalent for large d problems of the Wilson renormalization group method [15]. We will illustrate the different approaches in the following sections where we present our results on the Mott transition in the Hubbard model in large dimensions. Throughout the paper, we take the half-bandwidth $D = 2t = 1$.

3. The Mott Transition at Half Filling

The schematic (from 2OPT) phase diagram of the Hubbard model at half filling in a fully frustrated lattice is shown in figure 1.

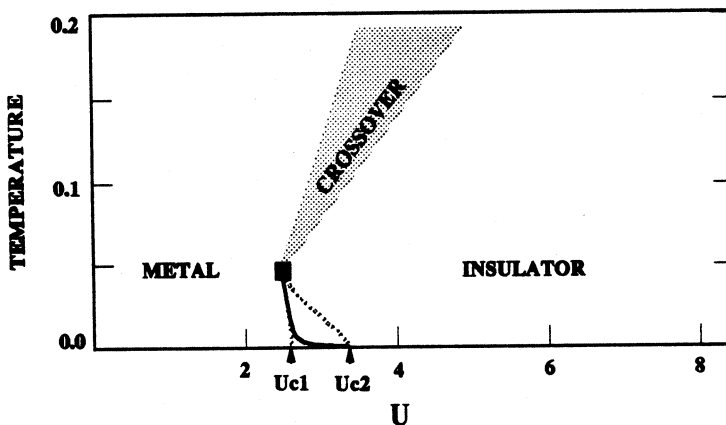


Fig.1 Phase diagram of the fully frustrated model.

At low temperature there are two phases a Fermi liquid metal characterized by a non zero density of states at zero energy and a paramagnetic insulator with a gap in the one particle excitation spectra. The metallic solution disappears at the dotted line ending at U_{c2} , while the insulating solution persists down to the dotted line ending at U_{c1} . There is a region enclosed by the lines $U_{c1}(T)$ and $U_{c2}(T)$, where both the metallic and the insulating solutions are allowed. Within this region, there is a first order boundary where the two very different solutions cross in free energy, and several quantities such as the specific heat, the susceptibility, the number of doubly occupied sites experience

a jump. The first order line has a negative slope indicating that the paramagnetic insulating phase has a higher entropy than the metallic phase. The line ends in an second order critical point, above which there is a smooth crossover between a metallic and an insulating regime.

At $T = 0$, we have shown using ED [14] that the metallic state is lower in energy than the paramagnetic insulator and therefore the first order line ends in a $T = 0$ second order quantum critical point (denoted U_{c2} in the figure). The ED and QMC method confirmed that the qualitative phase diagram obtained from 2OPT is correct, with only the values of U_{c1} and U_{c2} slightly reduced. With ED we obtained $U_{c1} \approx 2.15$ and $U_{c2} \approx 3.05$. For comparison notice that the Hubbard III approximation gives $U_{c1} = 1.73$, and the Brinkman-Rice approach limit gives $U_{c2} \approx 3.3$. The metallic solution is characterized by a narrow quasiparticle peak at the Fermi energy with a width e_F^* that goes to zero as $U_c - U$; plus two high energy incoherent features at $\pm \frac{U}{2}$. The magnetic phases of the models are displayed in figure 2. On bipartite (non frustrated) lattices the onset of Neel order preempts the Mott transition. We demonstrate this by calculating the Neel temperature of the Bethe lattice (dotted line). In this case one can understand the insulating phase by continuing the Slater insulator from the small U regime to the large U regime.

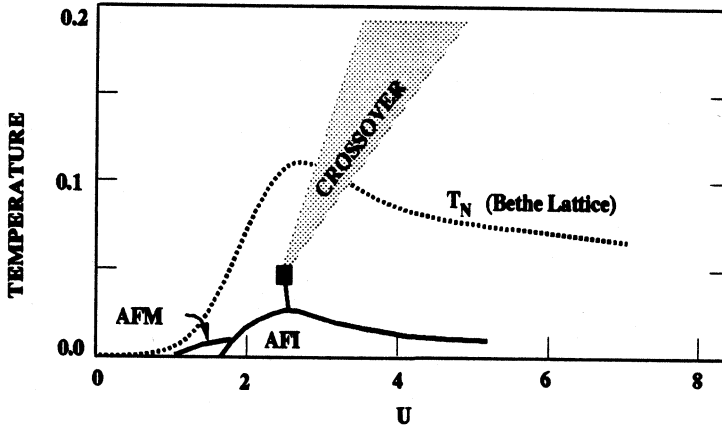


Fig.2 Phase diagram with magnetic phases of the models discussed in the text. The dotted line is the Neel temperature on the Bethe lattice. The solid lines give the phase diagram of the TSFF model.

As the degree of frustration is increased, the Neel temperature is reduced. In particular for parameters $t_1^2 = 0.75t^2$, $t_2^2 = 0.25t^2$, it falls below the 2nd order critical point and the first order transition becomes relevant, realizing Mott's scenario. Therefore we find that in a partially frustrated model (TSFF), the phase diagram features both a paramagnetic metal insulator transition at intermediate temperatures, and a Neel ordered phase at low temperatures. A small region of metallic antiferromagnetic phase is also obtained. To illustrate the numerical techniques employed, we calculate the behavior of various quantities as a function of U with the different methods. In figure 3 we plot the double occupation $\langle D \rangle$ as a function of U . There are two branches, corresponding to the metallic and insulating solutions at $T = 0$, which merge at $U_{c2} \approx 3$. They show the excellent agreement of the exact diagonalization algorithm and the 2OPT in all parameter range, except very close to the MIT point at U_c . The QMC data being at an inverse temperature $\beta = 32$, shows that the effect of the temperature is to reduce the double occupation on the metallic side. In the insulating side, the effect is negligible since in this case there are no small energy scales. At this temperature the coexistence region is very small, and the data shows a jump in $\langle D \rangle$ at $U \approx 2.4$. Notice that this result indicates that the Brinkman-Rice approach captures the singular part of $\langle D \rangle$,

but in addition we observe that this quantity does not vanish at the transition due to an additive non-singular part. We can thus parametrize $\langle D \rangle = 0.235(\frac{U_c - U}{U_c}) + 0.015$ near U_{c2} . Also note that the magnetic moment is obtained from the double occupation through the identity $\langle m_Z^2 \rangle = 1 - 2 \langle D \rangle$. Therefore, we find that the magnetic moment does not saturate at the transition [7, 8, 9, 10].

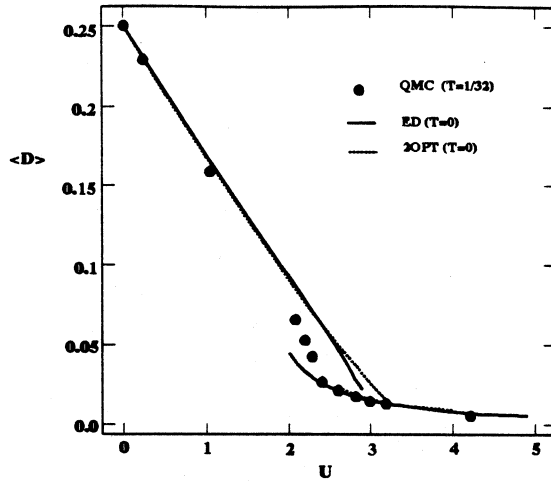


Fig.3 Double occupation as a function of the interaction U .

We also compare the value for the quasiparticle residue Z (inverse mass enhancement) as a function of U from the exact diagonalization method and the 2OPT (figure 4). For a small value of U the latter becomes exact, at an intermediate range they coincide and as the critical point is approached the exact diagonalization method, that treats the interaction non-perturbatively, becomes more accurate. Using the projective self consistent method we obtained $U_c \approx 3.05$. Notice that the Z vs. U plot is linear for a wide range of the interaction. The mass renormalization in the limit of infinite dimensionality is identical to the quasiparticle weight. The critical behavior of the renormalized mass is thus $\frac{m^*}{m} = Z^{-1} \approx 0.91(1 - (\frac{U}{U_c}))^{-1}$ in agreement with the Brinkman-Rice picture. We can define then the useful scale $e_F^* = ZD$ that describes the width of the quasiparticle peak at the Fermi energy in the metallic phase.

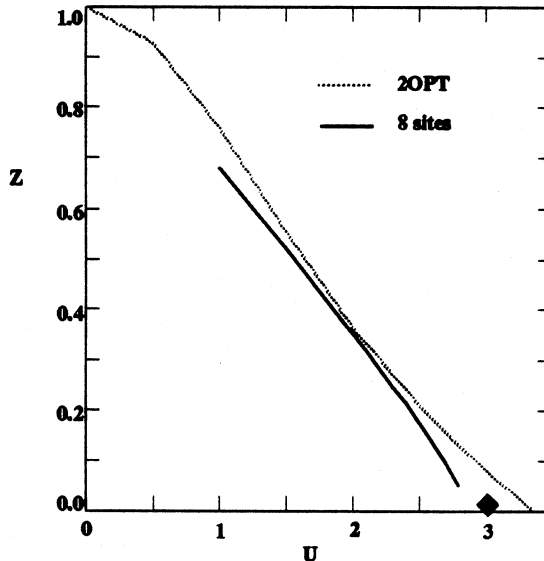


Fig.4 The quasiparticle weight Z as a function of interaction U .

In figure 5 we plot the inverse magnetic susceptibility χ_S^{-1} vs. U as obtained from the slope of the $\langle m_Z \rangle$ vs. h curves calculated by QMC simulations at an inverse temperature $\beta = 16$ [9, 10]. This quantity is given in units such that $\mu_B = 1$. Unlike the Brinkman-Rice approach this quantity remains finite at the transition due to the existence of a non-zero superexchange constant $J = \frac{2t^2}{U} = \frac{D^2}{2U}$ in the uniform response. The numerical result can be parametrized according to an analytic expression [10]. We find $\chi^{-1} \approx 0.23(U_c - U)$ for the metallic phase, and $\chi^{-1} \approx J$ in the insulator phase (J is plotted for comparison).

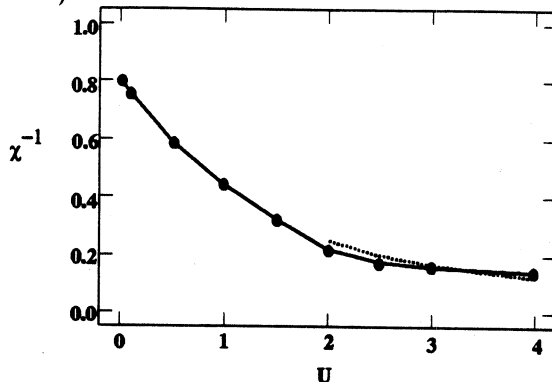


Fig.5 Inverse of magnetic susceptibility at $q = 0$ (solid dots) and the magnetic exchange J (dashed line) as a function of the interaction U .

We also obtained the Wilson ratio as a function of interaction U . This quantity is displayed in figure 6 and is derived from figures 4 and 5. It is found to vanish at the critical point since while the specific heat diverges as $\frac{1}{\epsilon_{F**}}$, the magnetic susceptibility is cut-off by $\min\{T^{-1}, J^{-1} = 2U/D^2\}$.

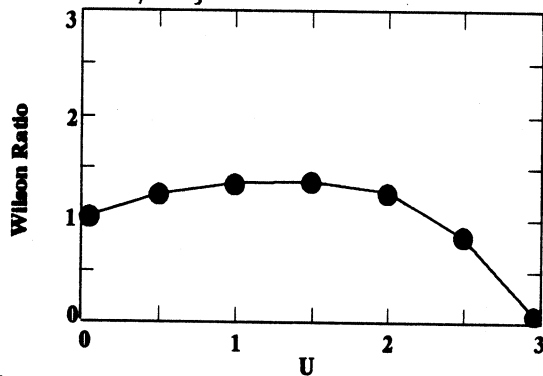


Fig.6 Wilson ratio as function of the interaction U .

In the region of the phase diagram around U_{c2} the Brinkman-Rice scenario for the destruction of the metal is realized. Surprisingly in the region around U_{c1} Hubbard's ideas regarding the closure of the Hubbard bands come to life. In figure 7 we plot the value of the Hubbard gap as a function of U in both the paramagnetic and the antiferromagnetic phase. As a definition for the magnitude of the gap we take twice the energy of the lowest energy pole of the Green function obtained from the exact diagonalization method. We show data extrapolated for finite size effects from exact diagonalization of systems of 3,5 and 7 sites. A $1/N_{sites}$ scaling behaviour is assumed. The results indicate that, following the insulating solution, the paramagnetic gap closes at a value $U_{c1} \approx 2.15$. Even though the paramagnetic insulating phase is strictly unstable at zero temperature, it is relevant to very frustrated magnetic insulators.

4. The Mott Transition as a function of doping

It is interesting to investigate the Mott transition as a function of doping in the Hubbard model. We believe that away from half-filling and in the paramagnetic phase there is

only one solution of the mean field equations, and then we can investigate the behavior of various quantities as a function of filling factor.

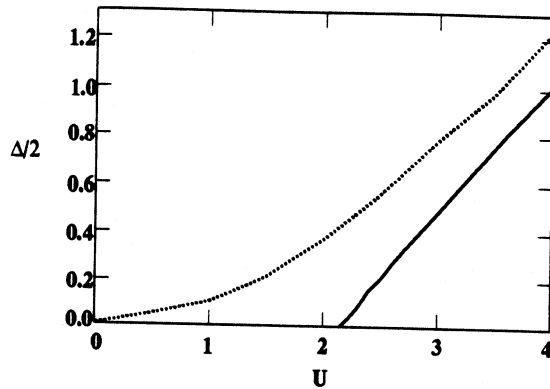


Fig.7 Antiferromagnetic (dotted line) and paramagnetic (solid line) gap as function of the interaction U .

We first show in figure 8, the particle occupation as a function of the chemical potential as obtained from QMC at $\beta = 16$. We note that the slope of the curve, i.e. the compressibility goes to zero at $\mu = 0$ as U_c is approached. For bigger values of U , we have a vanishing compressibility characteristic of an insulating state. It displays a gap equal to $U - 2D$ which compares very well with the results for the size of the gap from the exact diagonalization method (figure 7). Notice that for $U > U_c$ the $\delta vs. \mu$ curves approach half filling ($\delta = 0$) with a finite slope.

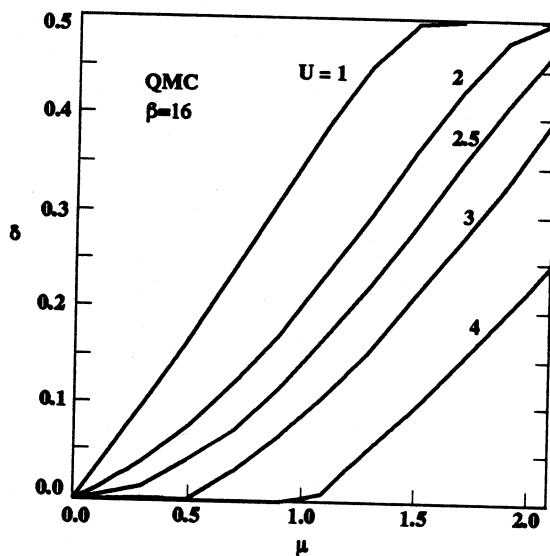


Fig.8 Particle number versus the chemical potential for different values of the interaction U .

We also calculated the specific heat and spin susceptibility as a function of doping for the case $U = 3$. This places the system close to the Mott point, as it seems to be the case for compounds as $La_xSr_{1-x}TiO_3$ and the high T_C cuprates. These quantities are displayed in figure 9 and are obtained from QMC at $\beta = 32$. The specific heat is plotted in units of $\frac{\pi^2 k_B^2}{3} \rho^0$, with $\rho^0 = \frac{4}{\pi D}$; while the spin susceptibility is in units of $\frac{\mu_B^2}{D}$. These results compare rather well with the experiments of Tokura *et al.* on $La_xSr_{1-x}TiO_3$ [17].

The Wilson ratio $(\chi_s/\gamma)/(\chi_s^0/\gamma^0)$ as function of doping is derived from these quantities (figure 10). Notice that its value is consistently lower than the experimental value $R = 2$. Whether this is due to a shortcoming of the mean field theory or it is some interesting effect of the many orbital character of the experimental system is an open problem.

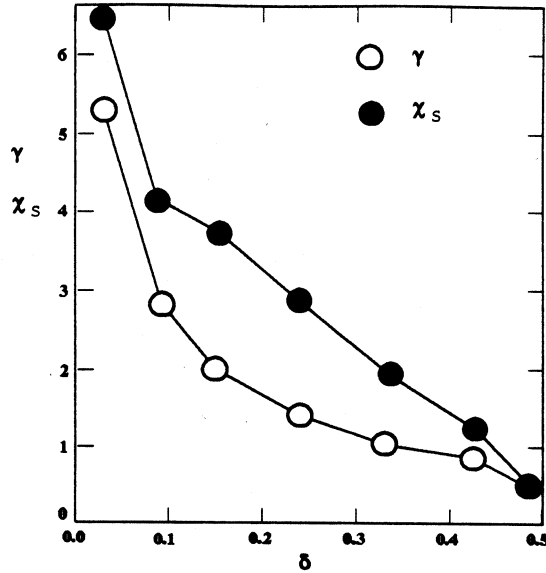


Fig.9 Specific heat and spin susceptibility as function of doping for $U = 3$.

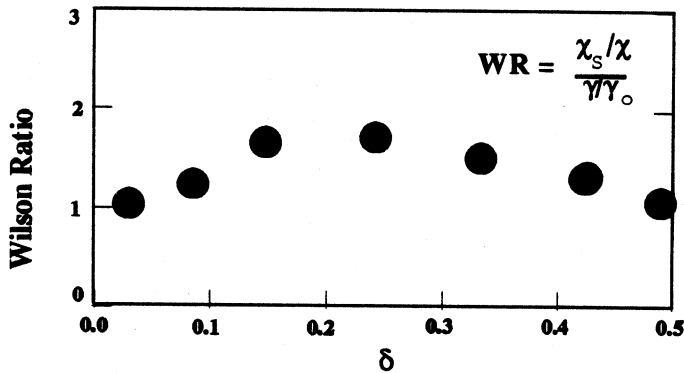


Fig.10 The Wilson ratio as function of doping for $U = 3$.

The optical conductivity of a correlated electron system at $T = 0$ can be parametrized by

$$\sigma(\omega) = \frac{\omega_P^{*2}}{4\pi} \delta(\omega) + \sigma_{reg}(\omega) \quad (8)$$

where the coefficient in front of the δ -function is the Drude weight and ω_P^* is the renormalized plasma frequency. In the presence of disorder $\delta(\omega)$ is replaced by a lorentzian of width Γ .

The kinetic energy is related to the conductivity by the sum rule

$$\int_0^\infty \sigma(\omega) d\omega = -\frac{\pi e^2}{2\hbar^2 a} \langle T \rangle = \frac{\omega_P^2}{4\pi} \quad (9)$$

where e is the electron charge and a the lattice constant. This expression is valid in any dimension.

The Drude part can be directly obtained in terms of the quasiparticle weight in the limit of $d \rightarrow \infty$. It can be shown that $\frac{\omega_P^{*2}}{4\pi} = \frac{2e^2}{3\hbar^2 a} DZ$.

In figure 11 we plot the kinetic energy $\langle T \rangle$ as a function of the doping δ , as obtained from QMC at $\beta = 16$.

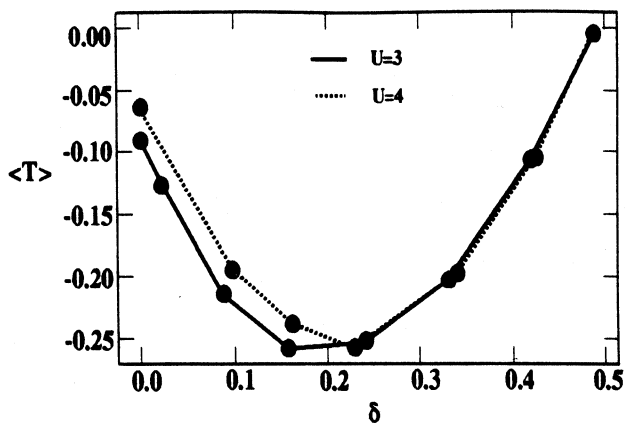


Fig.11 The kinetic energy as function of doping.

In figure 12 we plot the kinetic energy $\langle T \rangle$ as a function of the interaction U . This quantity is calculated at half filling in the paramagnetic metal and insulator phase, and also in the antiferromagnetic phase.

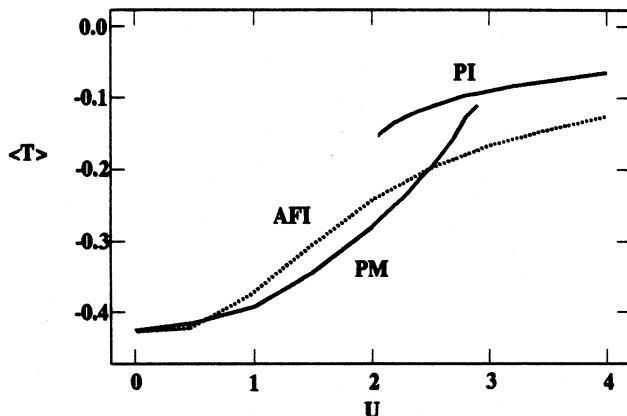


Fig.12 Kinetic energy in the paramagnetic (metal and insulator) and antiferromagnetic (insulator) phase as a function of the interaction U . Obtained from the ED method.

Therefore, the quantities $\langle T \rangle$ and Z , that are easily obtained within the present scheme, can be utilized to assess the validity of a simple one band Hubbard model to describe the low energy part of the optical conductivity of metal oxides.

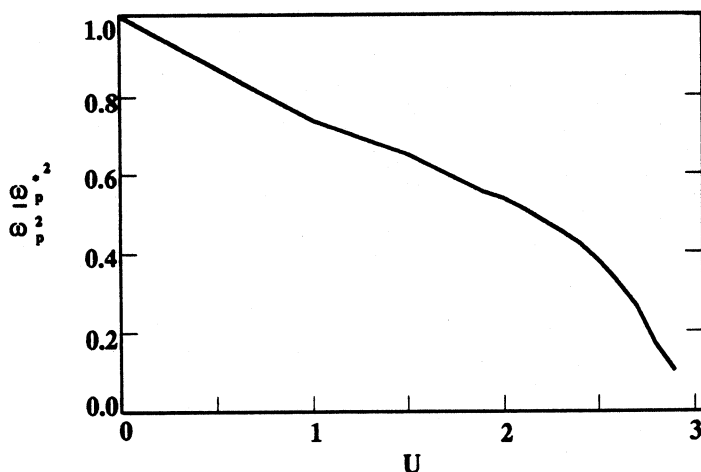


Fig.13 Ratio of the Drude part to the total spectral weight as a function of the interaction U .